Extending the diabatic surface layer wind shear profile for offshore wind energy

Holtslag, M. C.; Bierbooms, W. A A M; van Bussel, G. J W

DOI
10.1016/j.renene.2016.08.031

Publication date
2017

Document Version
Final published version

Published in
Renewable Energy

Citation (APA)
Holtslag, M. C., Bierbooms, W. A. A. M., & van Bussel, G. J. W. (2017). Extending the diabatic surface layer wind shear profile for offshore wind energy. *Renewable Energy*, *101*, 96-110. https://doi.org/10.1016/j.renene.2016.08.031

Renewable Energy 101 (2017) 96–110

Contents lists available at ScienceDirect

Renewable Energy

journal homepage: www.elsevier.com/locate/renene

Extending the diabatic surface layer wind shear profile for offshore wind energy

M.C. Holtslag*, W.A.A.M. Bierbooms, G.J.W. van Bussel

Faculty of Aerospace Engineering, Technical University Delft, The Netherlands

ARTICLE INFO

Article history:
Received 26 January 2015
Received in revised form
3 February 2016
Accepted 10 August 2016
Available online 31 August 2016

Keywords:
Wind profile
Boundary-layer meteorology
Monin-Obukhov similarity theory
Offshore atmosphere
Atmospheric stability
Wind energy

ABSTRACT

In this research the diabatic surface layer wind shear model is extended for offshore wind energy purposes to higher altitudes based on Gryning's wind profile and the resistance functions proposed by Byun. The wind profile is in theory applicable up to the boundary layer height, which is parametrized with the Rossby-Montgommery equation. The coefficient c of the Rossby-Montgommery equation is found to be stability dependent with decreasing values up to 0.04 for stable conditions and increasing values up to 0.17 for unstable conditions. The proposed shear profile has been validated with 1 year of offshore observation data, and a significant improvement in accuracy is found compared to traditional surface layer shear profiles or power laws. The influence of adopting this extended shear profile for wind energy is analysed in terms of the kinetic energy flux and blade root fatigue loads experienced by a wind turbine. It is found that, especially for stable conditions, results deviate significantly compared to using the traditional surface layer shear profile. The kinetic energy flux decreases by up to 15%.

1. Introduction

Wind shear is of great importance for wind turbine performance, both in terms of power production and fatigue loads. As such, it is crucial not only to accurately observe wind shear in resource assessment, but also to accurately prescribe wind shear in wind turbine design. Commonly used wind profiles in wind energy are either empirical by nature (power laws, as used in for example IEC guidelines [21] [22]) or valid close to the surface (diabatic surface layer wind profiles, based on Monin-Obukhov similarity theory [25,26]). State of the art multi-megawatt wind turbines however operate at heights well above the surface layer, thus it becomes necessary to incorporate a wind shear profile in wind energy research that is valid up to at least 150–200 m height or higher, depending on wind turbine characteristics. The validity of mentioned diabatic surface layer wind shear profiles up to such heights is questionable since they are applicable in the surface layer only [35]. It is thus needed to extend commonly used wind profiles up to heights above the surface layer.

Extrapolation of wind shear profiles to higher altitudes is not a novelty on its own, since already in the 1960's similar research was performed by Refs. [4] and [5]. These extended wind profiles however where typically derived for simplified atmospheric conditions in absence of stratification effects. In a recent study, however, Gryning derived a theoretic wind shear profile that covers the entire boundary layer [14], with specific parametrizations of the wind profile for stable and unstable stratifications. This profile has been validated in literature for onshore and coastal sites [14,29,32]. The offshore validation presented by Ref. [32] however is executed based on observations up to 116 m at most, which is too limited in scope of the dimensions of state of the art wind turbines. Besides, the two sites considered in Ref. [32] are located relatively close to the shore with a coastal distance of 18 km, hence the applicability of the wind profile for far offshore sites is unknown.

A recurring aspect of numerous studies related to atmospheric stability, wind shear and wind energy is that stability is classified in specific arbitrarily defined classes. Examples found in literature show a division of stability in three [15], four [28], five [37] or seven [33] stability classes, however, there is no physics based argument for the specific classifications adopted in these studies. In studies where Gryning's wind profile has been validated stability classes are also used (seven classes are considered in Refs. [14,29] and [32]. In a recent study [20], assessed the influence of adopting a continuous stability distribution instead of specific stability classes in wind turbine fatigue simulations and found differences in the simulated wind turbine fatigue loads up to 13%. As such, it is

* Corresponding author. Kluyverweg 1, 2629 HS, Delft, The Netherlands.
E-mail address: m.c.holtslag@tudelft.nl (M.C. Holtslag).

http://dx.doi.org/10.1016/j.renene.2016.08.031
0960-1481/

beneficial to parametrize an extended wind profile as a continuous functions of atmospheric stability.

To properly validate wind profiles up to heights relevant for state of the art wind turbines, one requires wind speed observations at high altitudes, which are traditionally obtained with tall meteorological masts [36]. Advances in LIDAR technology however [34] allow for wind observations above the surface layer without the need to construct such a meteorological mast, which is especially useful offshore or for complex terrain. The recent construction of a meteorological mast 85 km offshore in the Dutch North Sea area [19], including LIDAR observation data up to 315 m height, provides a unique opportunity to validate Gryning's wind profile for a far offshore site up to heights relevant for state of the art wind turbines.

The aim of this study is twofold. First of all we aim to parametrize and validate Gryning's wind profile for a specific far offshore site, elaborated upon in Section 3.1, up to heights relevant for wind energy purposes. In contrary to similar previous studies, we parametrize the wind profile as a continuous function of stability, and prevent the parametrization based on arbitrary stability classes. Although Gryning's wind profile is in theory valid for the entire boundary layer, we do not aim to validate the wind profile up to the top of the boundary layer. This is decided since the boundary layer height is typically much higher as the maximum blade tip height of a wind turbine, unless the boundary layer is very shallow. The second aim of this study is to assess if adopting either Gryning's wind profile or the diabatic surface layer wind profile in wind turbine simulations results in a different wind turbine response. In this paper we consider the wind turbine response in terms of power production as well as fatigue loads. Combined this should result in a practical and implementable extended wind shear profile for wind energy purposes, and it shows if indeed it is necessary to include such an extended wind profile in wind energy.

2. Derivation and parametrization of the extended wind shear model

We consider in this research the wind profile proposed by Gryning, and for sake of clarity we show the derivation in Section 2.1. Afterwards the theoretic wind profile is parametrized in Sections 2.2 and 2.3, and the parametrization adopted in this paper deviates from the parametrization considered in Ref. [14]. This allows us to show in detail which specific differences we adopt in the formulation of the extended wind profile, and we will also show the sensitivity of the wind profile to specific parameters. Unless stated otherwise, the equations and derivations are taken from Ref. [14].

2.1. Theoretic derivation of the wind shear profile

Based on dimensional analysis, wind shear in terms of the gradient $\partial\overline{U}/\partial z$ depends on a velocity scale υ and a local length scale l as

$$\frac{\partial \overline{U}}{\partial z} = \frac{\upsilon}{l} \tag{1}$$

Following Monin-Obukhov theory [25,26], one adopts the surface friction velocity u_{*0} as relevant velocity scale, assumed to be constant close to the surface, and the height z as relevant local length scale. Incorporating the definition of the dimensionless wind gradient ϕ_M to account for stability effects (see Ref. [6] or [35]) one finds

$$\frac{\partial \overline{U}}{\partial z} = \frac{u_{*0}\phi_M}{\kappa z} \tag{2}$$

where κ is the von Karman constant, assumed to be 0.4 [17]. The principle arguments proposed by Gryning are that in the atmospheric boundary layer the friction velocity decreases linearly with height, and that the local length scale l can be decomposed into a summation of three specific length scales. These three specific length scales correspond to a local surface layer length scale (assumed to be ϕ_M/z, similar as in surface layer scaling), a local middle layer length scale (assumed to be $1/l_{ML}$, which has to be parametrized) and a local upper layer length scale (assumed to equal $1/[h - z]$, where h is the boundary layer height). Incorporating these principle arguments in Equation (1), and taking into account the von Karman constant, results in

$$\frac{\partial \overline{U}}{\partial z} = \frac{u_{*0}}{\kappa}\left[1 - \frac{z}{h}\right]\left(\frac{\phi_M}{z} + \frac{1}{l_{ML}} + \frac{1}{h-z}\right) \tag{3}$$

In surface layer scaling it is assumed that the dimensional wind gradient is a universal function of stability in terms of ζ, where ζ is defined as

$$\zeta = \frac{z}{L} = -\frac{z\kappa g\left[\overline{w'\theta_v'}\right]_s}{u_{*0}^3\overline{\theta_v}} \tag{4}$$

Here L is the Obukhov length, g is the gravitational acceleration, $(\overline{w'\theta_v'})_s$ is the turbulent flux of virtual potential heat at the surface and θ_v is the virtual potential temperature. The dependence of ϕ_M on stability has been studied extensively in literature, and the Kansas experiment is likely the most well-known study [6,16], though more recent studies are shown in Refs. [1] and [10]. For unstable conditions one typically considers either the Businger-Dyer formulation [6] or the so called Free-Convection formulation [27], respectively

$$\phi_M = [1 - \gamma_{BD}\zeta]^{-1/4} \tag{5}$$

$$\phi_M = [1 - \gamma_{FC}\zeta]^{-1/3} \tag{6}$$

with $\gamma_{BD} = 19.3$ [17] and $\gamma_{FC} = 12.87$ [12]. For stable conditions one typically considers the Businger-Dyer formulation [6] or the formulation of Holtslag [39], respectively

$$\phi_M = 1 + \beta\zeta \tag{7}$$

$$\phi_M = 1 + \zeta[a + b\,[\exp(-d\zeta)[1 + c - d\zeta]]] \tag{8}$$

with $\beta = 6$ [17], and the coefficients a, b, c and d are respectively 1, 2/3, 5 and 0.35 [3]. The shown functions of ϕ_M all become one for neutral conditions where $\zeta = 0$. Integration of Equation (2) with respect to height results in the diabatic surface layer profile

$$\overline{U}(z) = \frac{u_*}{\kappa}\left[\ln\left(\frac{z}{z_0}\right) - \Psi(\zeta) + \Psi(\zeta_0)\right] \tag{9}$$

where z_0 is the aerodynamic roughness length, $\zeta_0 = z_0/L$ and Ψ is a stability correction function, which originates from Ref. [27].

$$-\int_{\zeta_0}^{\zeta}\frac{1-\phi_M}{\zeta}\,d\zeta = -\Psi(\zeta) + \Psi(\zeta_0) \tag{10}$$

The choice of adopting specific ϕ_M-functions in this research thus has an impact when deriving the extended wind profile, because of the required integration of Equation (3) (the integration results in multiple terms, not just Ψ as obtained for the surface layer wind profile). Following [14]; the Free-Convection formulation is adopted for unstable conditions, and the Businger-Dyer formulation is adopted for stable conditions, to derive the extended wind shear profile. Since two specific ϕ_M-functions for stable and unstable conditions are selected, also the stability correction functions typically found in surface layer scaling shear profiles are set. For respectively stable and unstable conditions these are

$$\Psi(\zeta) = -\beta\zeta \tag{11}$$

$$\Psi(\zeta) = \frac{3}{2}\ln\left(\frac{x^2+x+1}{3}\right) - \sqrt{3}\arctan\left(\frac{2x+1}{\sqrt{3}}\right) + \frac{\pi}{\sqrt{3}} \tag{12}$$

where $x = [1-\gamma_{FC}\zeta]^{1/3}$. Due to the linearity of Equation (11) one can write for stable conditions

$$\Psi(\zeta) = \frac{z}{h}\Psi(\zeta_h) \tag{13}$$

where $\zeta_h = h/L$. Both Ψ-functions are zero for neutral conditions. Integration of Equation (3) with respect to height, and assuming $z_0/h = 0$, leads to the following extended shear profile for respectively stable and unstable conditions

$$\overline{U}(z) = \frac{u_{*0}}{\kappa}\left[\ln\left(\frac{z}{z_0}\right) + \frac{1}{2}\left[2-\frac{z}{h}\right]\left[\frac{z}{h}\frac{h}{l_{ML}} - \Psi(\zeta)\right]\right] \tag{14}$$

$$\overline{U}(z) = \frac{u_{*0}}{\kappa}\left[\ln\left(\frac{z}{z_0}\right) - \Psi(\zeta) + \Psi(\zeta_0) + \frac{z}{h}\left[1 - \frac{3}{2}\frac{x_z^2 - x_0^2}{x_z^3 - 1}\right] + \frac{1}{2}\left[2-\frac{z}{h}\right]\frac{z}{h}\frac{h}{l_{ML}}\right] \tag{15}$$

where the subscripts z and 0 correspond to using respectively z and z_0 in x. Note that one could rewrite the term $z/h\ h/l_{ML}$ in these equations, but this is not done since a parametrization of h/l_{ML} will be derived. Besides, by incorporating Equation (13) in combination with the assumption that $z_0/h = 0$, there is no $\Psi(z_0/L)$-term in the shear profile for stable conditions.

2.2. Parametrization of h/l_{ML}

From here on we will deviate from the parametrization adopted by Ref. [14]. For the parametrization of l_{ML} we consider the geostrophic wind speed at the top of the boundary layer. A common expression for the geostrophic wind is obtained for barotrophic, stationary conditions as [5,43].

$$G = \frac{u_{*0}}{\kappa}\sqrt{\left[\ln\left(\frac{u_{*0}}{fz_0}\right) - B(\mu)\right]^2 + A^2(\mu)} \tag{16}$$

where G is the geostrophic wind speed, f is the Coriolis parameter, A and B are the resistance functions that will be parametrized in Section 2.3 and μ is the dimensionless stability parameter u_{*0}/fL. It is recognised however that Equation (16) is invalid if the boundary layer height h is not uniquely defined by μ alone, and in practice h also depends on other processes not taken into account in μ, such as entrainment and the vertical wind speed at the top of the boundary layer [7,43]. As such, an alternate formulation of Equation (16) is proposed in Ref. [43] where the boundary layer height h is a unique variable, which results in (see Equation (15) of [43].

$$G = \frac{u_{*0}}{\kappa}\sqrt{\left[\ln\left(\frac{h}{z_0}\right) - B\left(\frac{h}{L}\right)\right]^2 + A^2\left(\frac{h}{L}\right)} \tag{17}$$

Since the resistance functions now depend on the dimensionless parameter h/L instead of μ, the parametrization of A and B will differ compared to using Equation (16) [7]. Evaluating Equations (14) and (15) at $z = h$ and combining with Equation (17) yields expressions for h/l_{ML}

$$\frac{h}{l_{ML}} = 2\left[\sqrt{\left[\ln\left(\frac{h}{z_0}\right) - B\left(\frac{h}{L}\right)\right]^2 + A^2\left(\frac{h}{L}\right)} - \ln\left(\frac{h}{z_0}\right)\right] + \Psi\left(\frac{h}{L}\right) \tag{18}$$

$$\frac{h}{l_{ML}} = 2\left[\sqrt{\left[\ln\left(\frac{h}{z_0}\right) - B\left(\frac{h}{L}\right)\right]^2 + A^2\left(\frac{h}{L}\right)} - \ln\left(\frac{h}{z_0}\right) + \Psi\left(\frac{h}{L}\right) - \Psi\left(\frac{z_0}{L}\right) - \left[1 - \frac{3}{2}\frac{x_h^2 - x_0^2}{x_h^3 - 1}\right]\right] \tag{19}$$

where the subscript h denotes the usage of h/L instead of z/L in x.

For sake of clarity, the shear profile is rewritten as

$$\overline{U}(z) = \frac{u_{*0}}{\kappa}\left[\ln\left(\frac{z}{z_0}\right) + \Upsilon + \Omega\right] \tag{20}$$

where the last term is similar in notation for stable and unstable conditions and given by

$$\Omega = \frac{z}{h}\left[2-\frac{z}{h}\right]\left[\sqrt{\left[\ln\left(\frac{h}{z_0}\right) - B\left(\frac{h}{L}\right)\right]^2 + A^2\left(\frac{h}{L}\right)} - \ln\left(\frac{h}{z_0}\right)\right] \tag{21}$$

and all remaining terms are combined into a closing term. For stable conditions no terms remain due to the linearity of the stability correction function. We therefore find for respectively stable and unstable conditions

$$\Upsilon = 0 \tag{22}$$

$$\Upsilon = \frac{z}{h}\left[2-\frac{z}{h}\right]\left[\Psi\left(\frac{h}{L}\right) - \Psi\left(\frac{z_0}{L}\right)\right] - \left[\Psi\left(\frac{z}{L}\right) - \Psi\left(\frac{z_0}{L}\right)\right] + \frac{3}{2}\frac{z}{h}\left[\left[2-\frac{z}{h}\right]\frac{x_h^2 - x_0^2}{x_h^3 - 1} - \frac{x_z^2 - x_0^2}{x_z^3 - 1}\right] - \frac{z}{h}\left[1-\frac{z}{h}\right] \tag{23}$$

Combined, this wind shear profile is a function of the same parameters as the surface layer wind shear profile (thus z, z_0, L and u_{*0}), and three extra parameters: the boundary layer height h, and the two resistance functions A and B.

2.3. Parametrization of the resistance functions A and B

It is aimed in this study to define continuous functions for A and B, as opposed to choosing distinct values for a group of stability conditions as is done in Ref. [29]. The resistance functions A and B are parametrized following [7]. Note that [7] has a reversed definition of A and B compared to [43] and [14]; and here the notation of [43] is used in line with Equation (17). This results in

$$A = \frac{q+1}{q}\frac{\kappa u_{*0}}{fh} \tag{24}$$

$$B = \frac{p+1}{p} - \Psi\left(\frac{z_0}{L}\right) - \frac{\Psi\left(\frac{h}{L}\right)}{p} + \frac{p+1}{p\frac{h}{L}}\left[\Gamma\left(\frac{h}{L}\right) - \Gamma\left(\frac{z_0}{L}\right)\right] \tag{25}$$

where p and q are coefficients that vary between 1 and 3 (with $q = 1$ if the friction velocity decreases linearly with height and $p = 1.5$ for neutral conditions) and Γ is the integral of the stability correction function

$$\Gamma\left(\frac{h}{L}\right) = \int \Psi\left(\frac{h}{L}\right) d\frac{h}{L} \tag{26}$$

In absence of a proper parametrization of p as a function of stability we assume $p = 1.5$. For stable and unstable conditions Γ equals respectively

$$\Gamma\left(\frac{h}{L}\right) = \frac{1}{2}\frac{h}{L}\Psi\left(\frac{h}{L}\right) \tag{27}$$

$$\Gamma\left(\frac{h}{L}\right) = \frac{h}{L}\left[\Psi\left(\frac{h}{L}\right) - 1\right] - \frac{3}{2}\frac{x_h^2}{\gamma_{FC}} + \frac{31}{16\gamma_{FC}} \tag{28}$$

Combined this results for stable and unstable conditions respectively in

$$B = \frac{p+1}{p} + \frac{1}{2}\frac{p-1}{p}\Psi\left(\frac{h}{L}\right) - \Psi\left(\frac{z_0}{L}\right) \tag{29}$$

$$B = \frac{3}{2}\frac{p+1}{p}\frac{x_h^2 - x_0^2}{x_h^3 - 1} + \Psi\left(\frac{h}{L}\right) - \Psi\left(\frac{z_0}{L}\right) \tag{30}$$

where again it is assumed that $z_0/h = 0$. For neutral conditions these equations match, since

$$\lim_{L\to\infty} \frac{x_h^2 - x_0^2}{x_h^3 - 1} = \frac{2}{3} \tag{31}$$

We thus find for neutral conditions $B = 1.67$, and A is a function of the dimensionless parameter u_{*0}/fh.

With the above parametrization, the wind profile is a function of z_0, h, L and u_{*0}. To provide insight, we perform a brief sensitivity study to assess the sensitivity of the theoretic wind shear profile to these four parameters. Results are shown in Fig. 1, where the solid line in the four separate panels is the same reference wind profile for neutral conditions with $z_0 = 10^{-4}$ m, $h = 250$ m and $u_{*0} = 0.3$ m s^{-1}. With respect to the surface roughness it is found that the magnitude of the wind speed changes as a function of the surface roughness (i.e., for a lower surface roughness the wind speed increases), but in principle there is merely a shift in the profile along the x-axes with little change in the local wind gradient $\partial\overline{U}/\partial z$ at a given height. Notice that not only the wind speed close to the surface, but also at the top of the boundary layer (in this example at 250 m height) is influenced by z_0, since the geostrophic drag law is a function of z_0 as well (see Equation (17)). If the boundary layer height changes the wind profile will substantially change as well, and for a shallower boundary layer the local wind gradient increases (i.e., the wind profile appears to be steeper at a given height). It is found that a change in boundary layer height from 250 m to 350 m height has little influence on the wind profile. In contrary, the wind profile is very sensitive if the boundary layer height changes from 250 m to 150 m. Besides, close to the surface (say in the lowest 20 m) the wind profile is not sensitive to h since for z << h the wind profile approximately simplifies to the (diabatic) surface layer wind profile.

The impact of stability is in line with the known stability dependence of the surface layer profile [35]. If the atmosphere becomes stable stratified wind shear increases, while wind shear decreases for unstable conditions. Besides, the wind speed at the top of the boundary layer is a function of stability as well due to the dependence of the resistance function B on stability. We find in Equation (29) that if the atmosphere becomes more stable stratified B will become increasingly more negative, and hence the geostrophic wind increases in Equation (17). The sensitivity of the wind profile to the friction velocity is relatively straight forward, and the wind increases substantially with increasing u_{*0}.

3. Observation data and determination of wind profile parameters

So far the extended wind profile has been derived and parametrized based on theoretic arguments, however, in practice typically not all required input parameters are available from observation data. In this study we aim to validate the extended wind profile for a specific far offshore site discussed in Section 3.1. Due to limitations in the available observation data (i.e., no direct observations of z_0, u_{*0}, L or h), we consider site specific parametrizations as discussed in Section 3.2. Subsequently, in Section 4 the wind profile will be validated for the same observation site.

3.1. Observation data

The applicability of the extended wind shear profile to describe wind shear far offshore will be assessed with aid of observation data obtained at the meteorological observation site IJmuiden, located 85 km offshore at N 52° 50.89′ E 3° 26.14′ in the Dutch North Sea area [41]. A detailed description of the meteorological mast and sensor specifications can be found in Refs. [19]; and in the current study we refrain from discussing sensor specifications in detail. Whereas in Ref. [19] only observations of the lowest 100 m of the atmosphere are used, in the current study we aim to apply the derived extended wind profile up to higher altitudes. As such we include observation data obtained with the LIDAR that is installed at the platform of the meteorological mast. The installed LIDAR is a Zephir 300, which is a continuous wave LIDAR, and it is set to observe wind speed and wind direction at 10 observation heights from 90 to 315 m height, with a 25 m observation height spacing. Besides the LIDAR observation data, we also use wind speed and wind direction observations obtained with cup anemometers and wind vanes at 27 and 58 m height, and temperature, humidity and air pressure observations obtained at 21 m height in combination with surface temperature observations obtained with a wave buoy (see Ref. [19] for details).

Atmospheric conditions have been observed starting at January 2012 until December 2015, however, it is found that for an extended period of time temperature data of the wave buoy is missing. It is therefore decided to consider exactly two years of observation data for the following assessments. Observations taken in 2012 are used to obtain a necessary parametrization of the boundary layer height h as discussed in Section 3.2. A separate year of observations, taken from the first of June 2014 until the end of May 2015 are used to validate the profile in Section 4. As such we have two independent datasets obtained at the same observation site that can be used to parametrize and validate Gryning's wind profile for the offshore site considered.

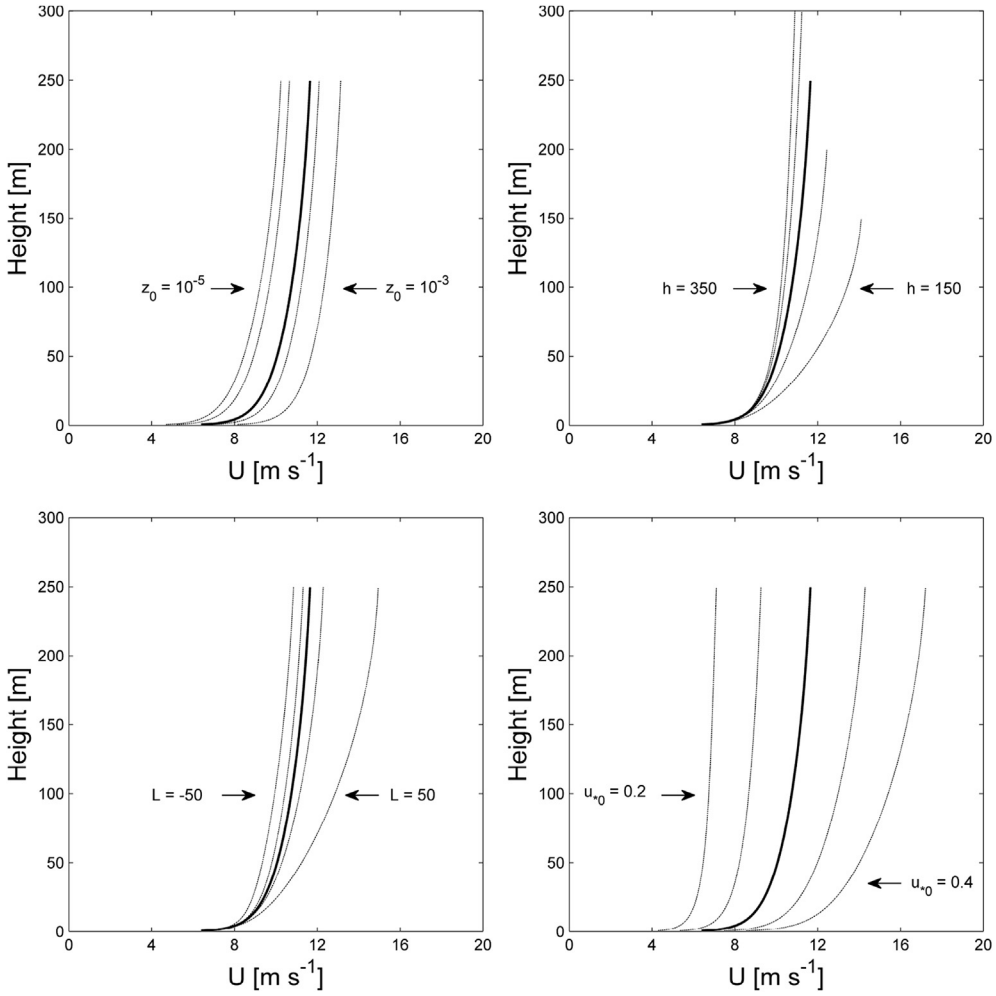

Fig. 1. Sensitivity of the theoretic wind shear profile to the aerodynamic roughness z_0 (upper left panel), the boundary layer height h (upper right panel), the Obukhov length L (lower left panel) and the surface friction velocity u_{*0} (lower right panel). The solid black lines in the four panels are all similar as a reference profile with $z_0 = 10^{-4}$ m, $h = 250$ m, $L = \infty$ and $u_{*0} = 0.3$ m s^{-1}.

3.2. Site specific parametrizations

The parametrized extended wind profile is a function of the aerodynamic roughness length, the friction velocity, atmospheric stability and boundary layer height, and neither of these parameters is directly observed at the site considered. As such we have to estimate the required parameters from the available observation data. In absence of observations of the turbulent heat and momentum flux sufficiently close to the surface, we follow [13] and estimate stability from the bulk Richardson number, which is defined as

$$RI = \frac{g\Delta\overline{\theta}_v \Delta z}{\overline{\theta}_v (\overline{U})^2} \tag{32}$$

Subsequently ζ is calculated as [13].

$$\begin{aligned} \zeta &= 10RI \quad \text{if RI} \le 0 \\ \zeta &= \frac{10RI}{1-5RI} \quad \text{if RI} \ge 0 \end{aligned} \tag{33}$$

The singularity at $RI = 0.2$ prevents calculation of ζ, thus for $RI > 0.2$ stability is not calculated. The conversion from ζ to L is discussed in detail in Ref. [19]. In the remaining analyses we will consider stability either in terms of L or in terms of $100/L$, similar to [14,29] and [32]. Since we consider offshore conditions, z_0 is parametrized with Charnock's equation [9].

$$z_0 = \alpha \frac{u_{*0}^2}{g} \tag{34}$$

with $\alpha = 0.012$ [28] and g is the gravitational acceleration of 9.81 m s^{-2}. The friction velocity is iteratively calculated, assuming validity of surface layer scaling in the lowest 27 m of the atmosphere (i.e., the lowest wind speed observation height), as

$$u_{*0}\left[\ln\left(\frac{zg}{\alpha u_{*0}^2}\right) - \Psi(\zeta)\right] = \kappa\overline{U}(z) \tag{35}$$

Where the Ψ-functions of Equations (11) and (12) are used. The observation dataset has no direct estimates of the boundary layer height h, hence we follow Gryning and consider the Rossby-Montgommery equation

$$h = c\frac{u_{*0}}{f} \tag{36}$$

where c has to be parametrized. Although, as discussed in Section

2.2, h is in reality dependant on other parameters as well, here we adopt Rossby number similarity theory and assume h is defined as a function of u_{*0}, f and L alone. Subsequently c will be parametrized as a function of stability.

As discussed before, it is aimed in this paper to parametrize the wind profile as a continuous function of stability. As such, in contrary to [29] and [32]; we also need a continuous parametrization of c as a function of atmospheric stability. To obtain this continuous parametrization we consider observation data obtained in 2012, and fit the theoretic extended wind profile to the observation data. All observations obtained at the meteorological measurement site are stored as 10-min mean observations. If for a given 10-min timestep any wind speed observation is missing in the observed wind profile up to 315 m height, the timestep is not considered for the parametrization of c. Besides, we filter for stationary conditions following [24] since Equation (3) is valid for stationary conditions [14]. After application of these filters a total dataset of 37623 observations remains, which equals approximately 71% of all data. The far majority of discarded data was not classified stationary following the criteria of [24]. The relative occurrence of unstable and stable conditions in the original and filtered dataset of 2012 is found to be similar (not shown in detail here), hence we expect the remaining data is representative despite the applied filter.

For each timestep only observation data at or below 27 m height are used to determine L and u_{*0}. As such it is decided not to include the 27 m height wind speed observations when fitting the wind profile to observation data, since this could result in self correlation [2]. Observations are grouped as a function of stability in terms of $100/L$, ranging from -5 to 2 with a 0.1 binsize. For each stability group the derived extended wind shear profile is fitted to the observation data, where h is estimated with Equation (36). The procedure is done with $c = 0.01$ to 0.50 with increments of 0.001, to find an optimal fit for the given stability group. The quality of the fit is assessed by computing the root mean square error (RMSE) between the modelled and observed wind speed, where the RMSE is calculated as

$$RMSE = \sqrt{\frac{1}{n}\left[\sum\left(\overline{U}_{fit}(z) - \overline{U}_{obs}(z)\right)^2\right]} \tag{37}$$

where $\overline{U}_{fit}(z)$ and $\overline{U}_{obs}(z)$ correspond to respectively the fitted and observed wind speed at height z, and n is the number of observation heights considered in the fit of the shear profile. We assume c is optimal for a given stability if the average RMSE of the fitted wind profiles is smallest. It is decided to fit the profile to observations up to 140 m height specifically. This is done since if either c or u_{*0} is very small, Equation (36) will estimate h to be low as well, which would prevent us from fitting the theoretic wind profile to several observations. We could raise this minimum boundary layer height up to 315 m height to cover all observations, however, it is recognised that for stable conditions the boundary layer can be shallow. The specified 140 m is thus a compromise, to fit the profile to several observations while also being able to parametrize c for (very) stable conditions. We have also done the same fitting procedure with a minimum boundary layer height of 250 m, which resulted in nearly the exact same parametrization for unstable and neutral conditions. The resulting optimal c-value as a function of stability is shown in Fig. 2, including an empirical fit to the obtained results.

It is clear that c depends on stability, and c equals approximately 0.15–0.20 for strong unstable conditions, approximately 0.09 for neutral conditions and slightly less then 0.05 for strong stable conditions. For situations where $100/L > 2$ m^{-1} it was found that c increases significantly again up to value's around 0.20, but due to a sharp increase in the RMSE these results are not considered to be appropriate. The empirical fit shown in Fig. 2 for stable and unstable conditions corresponds to respectively

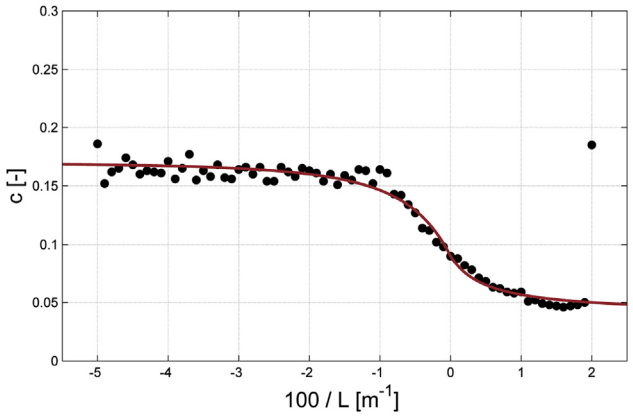

Fig. 2. Value of coefficient c as a function of stability where the theoretic wind profile has an optimal fit to the observation data, as calculated with Equation (37).

$$c = 0.04 + 0.05\left(1 + 2\frac{100}{L}\right)^{-1} \tag{38}$$

$$c = 0.17 - 0.08\left(1 - 0.5\frac{100}{L}\right)^{-3} \tag{39}$$

Which is forced to match for neutral conditions at $c = 0.09$. This provides a continuous parametrization of c as a function of stability, which has limiting values of 0.04 and 0.17 for extreme stable and unstable conditions. The results obtained for neutral and stable conditions are significantly smaller than proposed by Refs. [32]; who used $c = 0.15$ and $c = 0.13$ for respectively neutral and very stable conditions. It is possible that differences in characteristics between the sites considered in the current study and in either [29] or [32] cause a differences in the boundary layer height for similar surface conditions. This would result in a different parametrization of c for similar surface conditions. Besides, the parametrization of A and B in this study differs from values considered by Refs. [29] and [32]; which might cause a different parametrization of c to obtain proper fits of the extended wind profile to observation data. Due to the small value of c for stable conditions, it is possible that for stable conditions the boundary layer height is estimated with Equation (36) below 200 m height. This will constrain the applicability of the wind profile for wind energy purposes, which will be discussed in more detail in Section 5.

With a parametrization of c, the boundary layer height is a function of L, u_{*0} and f alone as expected from Rossby scaling [7]. As such, assuming a specific latitude, the extended wind shear profile is with the specified parametrizations a function of L and u_{*0} alone. The resulting profile will be validated in Section 4, however, we briefly assess the sensitivity of the resulting wind profile to L and u_{*0}. Results are shown in Fig. 3, in which the solid black lines in the four panels corresponds to the same situation (i.e., neutral conditions with $u_{*0} = 0.3$ m s^{-1}). With respect to stability it is found that if the atmosphere changes from unstable to neutral or stable conditions, the wind speed close to the surface increases, the local wind gradient $\partial\overline{U}/\partial z$ increases and the boundary layer height decreases. With respect to the friction velocity it is primarily found that the wind speed and boundary layer height increase with increasing u_{*0}, however, the local wind gradient shows little change as a function of u_{*0}. The non-dimensional wind profiles differ

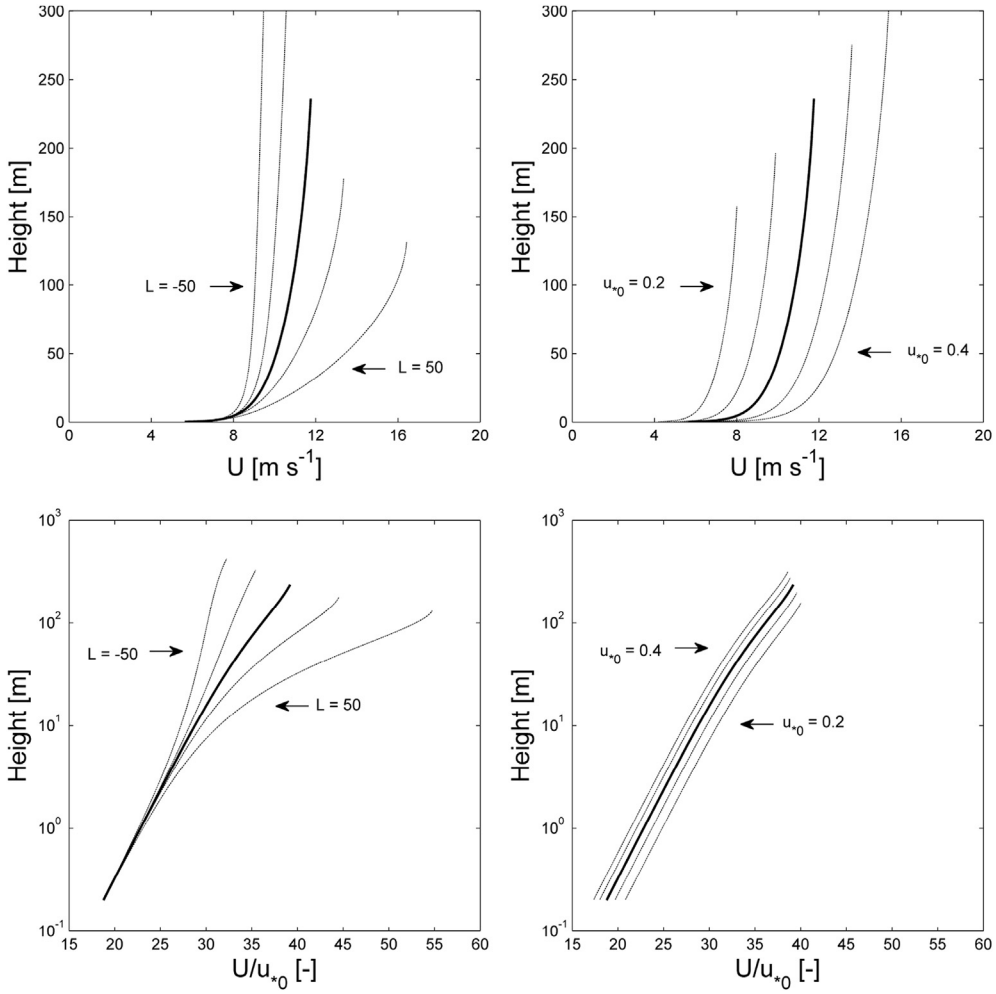

Fig. 3. Sensitivity of the parametrized wind shear profile to stability (left panels) and u_{*0} (right panels), where upper panels show the wind profile and lower panels show the non-dimensional wind profiles. The solid black lines are similar for the four panels and correspond to a reference wind profile for neutral conditions with $u_{*0} = 0.3$ m s^{-1}.

substantially as a function of stability, however, for a given stability the wind profiles nearly collapse (i.e., the lower right panel in Fig. 3 for neutral conditions). This is also the reason why in the following validation we consider non-dimensional wind profiles, since the absolute wind speed differs substantially as a function of u_{*0}. The non-dimensional profiles do not perfectly collapse since various parameters of the wind profile are still a function of u_{*0}. As shown in Ref. [28] this can be circumvented for the diabatic surface layer profile by introducing a stability-mean roughness length. In the derived extended wind profile both h and z_0 are a function of u_{*0}, hence a similar procedure is not applicable here.

In the following section we aim to validate the parametrized extended wind profile, and assess the performance of the extended wind shear profile compared to commonly used wind profiles in meteorology and wind energy.

4. Validation of the extended wind profile

To avoid validating the theoretic with the same data as was used for the parametrization, which would result in an overestimation of the accuracy of the wind profile, we consider a separate complete year of observation data. We use similar filters as described in the parametrization (i.e., no missing data in the observed wind profiles as well as stationary conditions), which results in 30469 observations (approximately 58% of all observations). This is substantially less as was found for 2012, used in the parametrization of c, primarily due to an increase in missing LIDAR wind speed observations. We therefore provide in more detail information about the amount of unstable, neutral and stable observations considered in the validation in Section 4.1. The various parametrizations proposed in the previous sections all allow the extended wind shear profile to be a continuous function of atmospheric stability. In principle there is thus no need to validate the wind profile for specific stability classes, however, for visualization purposes as well as for comparison purposes with literature, we will first validate the wind profile for specific stability classes. Once done, we also validate the profile for a continuous range of stability.

4.1. Validation with stability classes

The observation data is grouped with respect to stability, and we consider here a slightly modified version of the classification set used by Ref. [29] with a slight modification of the stable and very stable classes (see Table 1). The stable and very stable classes are on purpose modified to have similar absolute class boundaries as used for unstable and very unstable conditions, since there is no physics based argument to adopt different class boundaries for stable and unstable conditions. For each stability class we determine the average observed non-dimensional wind profile based on all observations where 0.1 m s^{-1} $\leq u_{*0} \leq$ 0.8 m s^{-1}. Next we determine the

Table 1
Overview of stability class characteristics used in Fig. 4.

Stability class [−]	Stability regime [m]	L (prof.) [m]	u_{*0} (prof.) [m s^{-1}]	Nr. of Obs. [−]
Very Unstable (VU)	$-100 \leq L < -50$	−69	0.33	5363
Unstable (U)	$-200 \leq L < -100$	−135	0.38	4412
Near Neutral Unstable (NNU)	$-500 \leq L < -200$	−284	0.38	2522
Neutral (N)	$\|L\| > 500$	−1336	0.35	2810
Near Neutral Stable (NNS)	$200 < L \leq 500$	296	0.34	1950
Stable (S)	$100 < L \leq 200$	141	0.26	1623
Very Stable (VS)	$50 < L \leq 100$	72	0.20	952

average of the inverse of the Obukhov length for each stability group, which will be used to calculate theoretic wind profiles. The theoretic wind profiles are forced to match the observations at 27 m height for each stability class, which provides an estimate of u_{*0} used to calculate the theoretic wind profiles. With L and u_{*0} calculated, the theoretic wind profiles and the observed wind profiles are shown in Fig. 4. The markers correspond to the average observed non-dimensional wind speed, the solid lines correspond to the extended wind profile and the dashed lines correspond to the surface layer wind profile with the Businger-Dyer and Free-Convection stability correction functions of Equations (11) and (12).

For (very) unstable conditions it is found that the surface layer wind profile corresponds well to the observations up to approximately 60 m height, but for higher altitudes the wind speed is underestimated. The extended wind profile overall has better agreement, especially for heights above 200 m, though in between 100 and 200 m height the extended wind profile also appears to slightly underestimate the observed wind speed. Do note however that the difference between the observed and modelled non-dimensional wind speed is in the order of $\overline{U}/u_{*0} \approx 0.5$ for the extended wind profile, which corresponds to wind speed differences less than 0.5 m s^{-1} for the majority of observations. It is also found that for unstable conditions the non-dimensional wind speed increases with height below 200 m height, while this

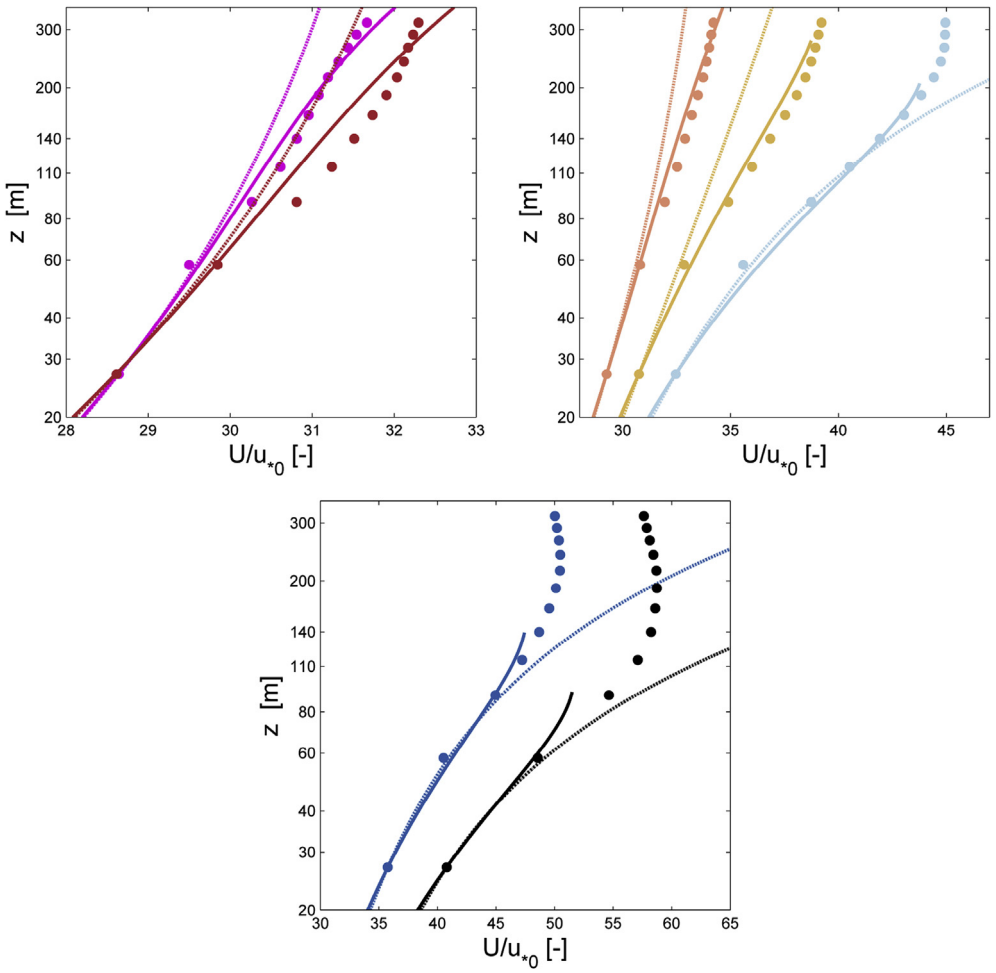

Fig. 4. Validation of the non-dimensional extended wind profile (solid lines) and the non-dimensional surface layer wind profile (dashed lines) compared to mean non-dimensional observed wind profile (markers) for various stability conditions. The upper left panel shows very unstable (VU, magenta) and unstable (U, dark red) conditions, the upper right panel shows near neutral unstable (NNU, light red), neutral (N, yellow) and near neutral stable (NNS, light blue) conditions and the lower panel shows stable (S, dark blue) and very stable (VS, black) conditions. (For interpretation of the references to colour in this figure legend, the reader is referred to the web version of this article.)

increase diminishes above 200 m (i.e., the observations appear to curve to the left above 200 m height). The extended wind profile however shows the opposite behaviour and above 200 m height there is an enhanced increase of the non-dimensional wind speed with height (i.e., the extended profile appears to curve to the right above 200 m height). The observations in Fig. 4 of [29] for unstable conditions show the same behaviour as the extended wind profile in Fig. 4 of paper, and also show a strong curve to the right. Besides, also for very unstable conditions (both in the current study as well as in Fig. 4 of [29] the observed wind speed appears to curve to the right above approximately 200 m height. It is therefore possible that the observations for unstable conditions in Fig. 4 of the current paper incorrectly show that the increase in wind speed with height above 200 m height diminishes.

For (near) neutral conditions in general similar results are found as for (very) unstable conditions, though with different orders of magnitude. For neutral and slightly unstable conditions the surface layer wind profile underestimates wind speeds above 60 m height whereas the extended wind profile has a substantial higher agreement with the average observed non-dimensional wind profile. For slight stable conditions however the surface layer performs well up to 140 m height, and for higher altitudes there is an overestimation of the wind speed. The extended wind profile again has high agreement with the observation data, though at 58 m height there seems to be a slight overestimation of the wind speed compared to the observations. It is found that at 190 m height, the extended wind profile slightly underestimates the non-dimensional wind speed by $\overline{U}/u_{*0} \approx 0.5$. The surface layer wind profile however causes an underestimation of $\overline{U}/u_{*0} \approx 1$ to 2.5 for respectively near neutral unstable and neutral conditions, and an overestimation of $\overline{U}/u_{*0} \approx 2$ for near neutral stable conditions. Notice as well that for neutral and slightly stable conditions the extended wind profile does not continue up to 315 m height since for the calculated values of L and u_{*0} the top of the boundary layer is determined below 315 m height. It is found that for near neutral stable conditions the average observed non-dimensional wind profile no longer increases with height above 250 m height. Although one could interpret this as an indirect observation of the boundary layer height, do note that here we average many observations, hence the observed boundary layer height is expected to vary a lot for the individual observations.

For (very) stable conditions result differ substantially compared to the previously discussed stability classes. First of all the average observations for both stable and very stable conditions show a wind maximum at respectively 200 and 160 m height. In Ref. [29] similar results are shown for very stable conditions, which might be an indication of the occurrence of low-level jets. For stable conditions the extended wind profile has a good agreement with the observation data, though there is a slight underestimation of the non-dimensional wind speed at 140 m height. For very stable conditions this underestimation is found at 90 m height all ready. The surface layer wind profile corresponds well to the observation data up to 90 m height for stable conditions, and up to 60 m height for very stable conditions, but there is a severe overestimation of the wind speed at higher altitudes. Especially at heights above 140 m the difference in the non-dimensional wind speed is in the order of $\overline{U}/u_{*0} \approx 5$ or larger, which can easily correspond to wind speed overestimations of more than 2 m s^{-1}.

For stable and very stable conditions it is found that the extended wind profile does not perform as good as for other stability classes, hence it is decided to examine these stable conditions in more detail. The observations for stable and very stable conditions are further classified as a function of the friction velocity to assess if the wind profile performs better for specific conditions. Results are shown in Fig. 5.

For $u_{*0} < 0.35$ m s^{-1} (the upper panels in Fig. 5), the extended wind profile and the surface layer wind profile nearly coincide up to 60 m height. At higher altitudes however the extended wind profile does not perform well, especially in close proximity of h, which is estimated to be below 150 m height. This shows that with the adopted parametrization of h, the extended wind profile does not define the wind shear profile at all heights relevant for wind energy purposes. There is thus a need to extend Gryning's wind profile up to heights above h for (very) stable conditions. For $u_{*0} > 0.35$ m s^{-1} (the lower panels in Fig. 5) the extended wind profile performs well for most observation heights, and substantially better compared to the surface layer wind profile. It is found, in agreement with [29]; that the surface layer wind profile with the Businger-Dyer stability correction function of Equation (11) severely overestimates wind shear above 50 m height. This is expected to be of importance when assessing the influence of wind shear on wind turbine performance, which is done in Section 5.

The extended wind profile typically performs poorly close to the top of the profile (i.e. for heights close to the estimations of h), which might have several causes. First of all, the parametrization of h could well be incorrect for specific individual observations, since the boundary layer height is a function of variables not considered in the parametrization adopted in the current research [7,43]. Second, it is assumed in Ref. [14] that the length scale of the wind gradient becomes 0 m in close proximity of the top of the boundary layer. In reality this is not necessarily true, as is shown for neutral conditions in Ref. [30]. As a last consideration, wind shear can be heavily influenced by the occurrence of low-level jets, which is not accounted for in the derivation of the wind profile. Despite the poor performance of the wind profile in close proximity of h, the general performance at lower altitudes is good and either equal or better compared to the surface layer wind profile.

4.2. Validation for stability as a continuous parameter

The extended shear profile so far has been validated for seven specific stability classes, however, the aim of this paper is to define and parametrize an extended wind shear profile that performs well for a continuous range of stability conditions, not for a group of stability conditions combined. It is decided to adopt a similar approach as was used for the parametrization of c in Section 3.2, hence stability conditions of $100/L$ ranging from -5 to 2 with a 0.1 binsize are considered. As such we consider here 71 narrow stability classes, compared to the 7 general classes used in the previous section, which serves as an approximation of stability on a continuous scale. For all observations of a stability bin the extended wind profile and several other wind profiles commonly used in wind energy are compared to the observed wind profiles, and for each observation the RMSE is calculated between the observed and theoretic wind shear profile. These profiles are the power law with a power coefficient of 0.14, following IEC guidelines for offshore conditions [22], a neutral logarithmic wind profile (i.e., Equation (9) without stability correction), and the diabatic surface layer wind profile similar as used in Ref. [19]. Combining Equation (10) with Equations (5)–(8) results in four Ψ-functions that we hereafter refer to as respectively Businger-Dyer and Free Convection (both for unstable conditions), and as Businger-Dyer and Holtslag (both for stable conditions). For unstable conditions the Businger Dyer and the Free Convection Ψ-functions equal respectively

$$\Psi(\zeta) = 2\ln\left(\frac{1+x}{2}\right) + \ln\left(\frac{1+x^2}{2}\right) - 2\arctan(x) + \frac{\pi}{2} \qquad (40)$$

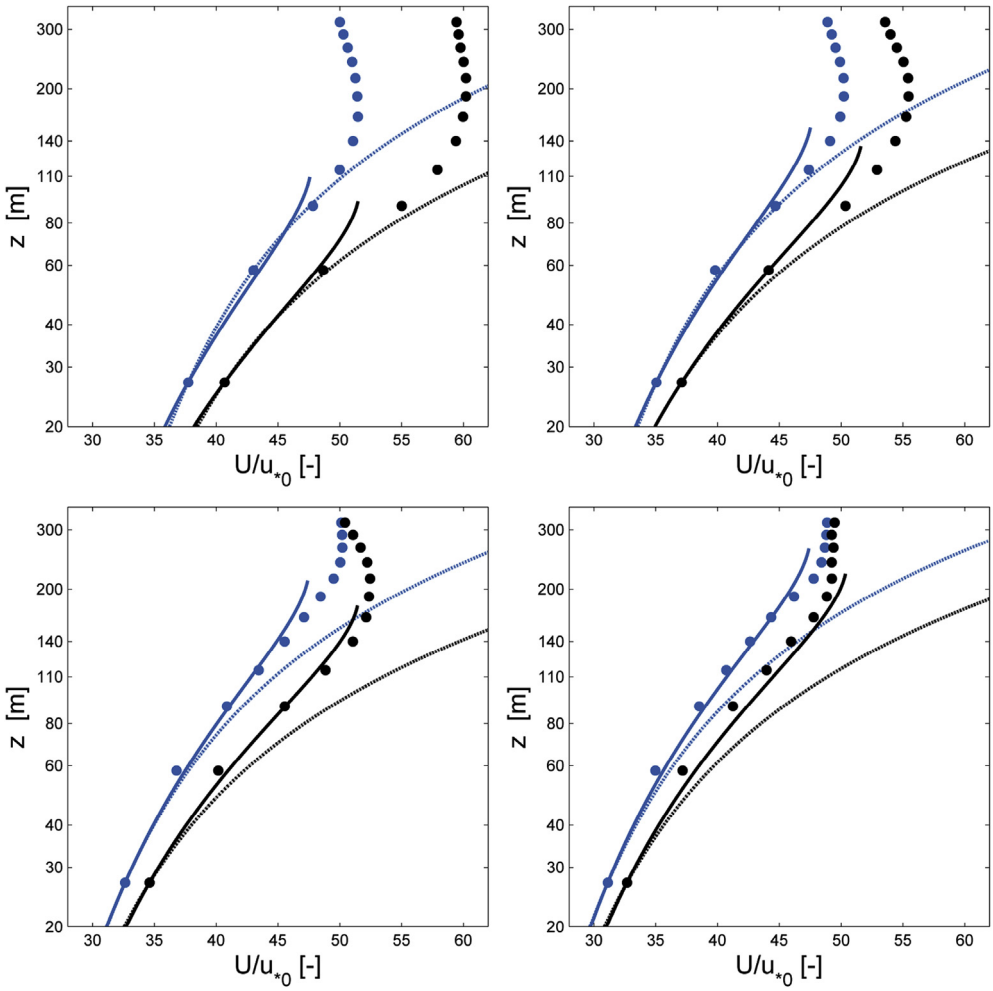

Fig. 5. Similar wind profiles as shown in Fig. 4 for stable (S, dark blue) and very stable (VS, black) conditions conditioned to u_{*0}. The panels corresponds to $0.15 \leq u_{*0} \leq 0.25$ (upper left panel), $0.25 \leq u_{*0} \leq 0.35$ (upper right panel), $0.35 \leq u_{*0} \leq 0.45$ (lower left panel) and $0.45 \leq u_{*0} \leq 0.55$ (lower right panel). (For interpretation of the references to colour in this figure legend, the reader is referred to the web version of this article.)

$$\Psi(\zeta) = 1.5 \ln\left(\frac{1+y+y^2}{3}\right) - \sqrt{3}\arctan\left(\frac{2y+1}{\sqrt{3}}\right) + \frac{\pi}{\sqrt{3}} \qquad (41)$$

where $x = (1 - \gamma_{BD}\zeta)^{1/4}$, $y = (1 - \gamma_{FC}\zeta)^{1/3}$, $\gamma_{BD} = 19.3$ [17] and $\gamma_{FC} = 12.87$ [12]. For stable conditions the Businger Dyer and the Holtslag Ψ-functions equal respectively

$$\Psi(\zeta) = -\beta\zeta \qquad (42)$$

$$\Psi(\zeta) = -a\zeta - b\left(\zeta - \frac{c}{d}\right)\exp(-d\zeta) - \frac{bc}{d} \qquad (43)$$

where $\beta = 6$ [17] and $a = 1$, $b = 2/3$, $c = 5$ and $d = 0.35$ [3]. Fig. 6 shows the average RMSE found as a function of stability for the various theoretic wind profiles.

For unstable conditions it is found that the extended wind profile performs approximately as good as the surface layer wind profiles with a stability correction. Only for near neutral conditions the extended wind profile starts to perform better compared to these specific surface layer wind profiles. The neutral surface layer wind profile performs less good for unstable conditions. Due to the absence of a stability correction the neutral surface layer wind profile overestimates wind shear. The power law performs very poor for unstable conditions since wind shear is strongly overestimated with the exponent of 0.14 considered here.

For stable conditions, the extended wind profile performs far better than any of the other shear profiles. Here it is found that the power law performs reasonably well, since wind shear is strong for stable conditions, which is also achieved when the power law wind profile is used with a power exponent of 0.14. Besides, the surface layer wind profile with the stability correction function of Holtslag performs substantially better compared to the Businger-Dyer correction function, in line with results shown in Ref. [19]. It is remarkable that the neutral surface layer wind profile also performs quite well for stable conditions compared to the surface layer wind profile with the stability correction of Holtslag. It is expected here that the neutral wind profile underestimates wind shear for stable conditions (especially close to the surface), while the wind profile including the correction function of Holtslag overestimates wind shear (especially at higher altitudes).

Combined, it is found that for all stability conditions considered in this assessment, the extended wind profile performs either as well as other wind profiles (for unstable conditions) or it performs better (for neutral and stable conditions). As such, incorporating the extended wind profile in wind turbine simulations will result in a better representation of atmospheric conditions for the far offshore site considered in the current research.

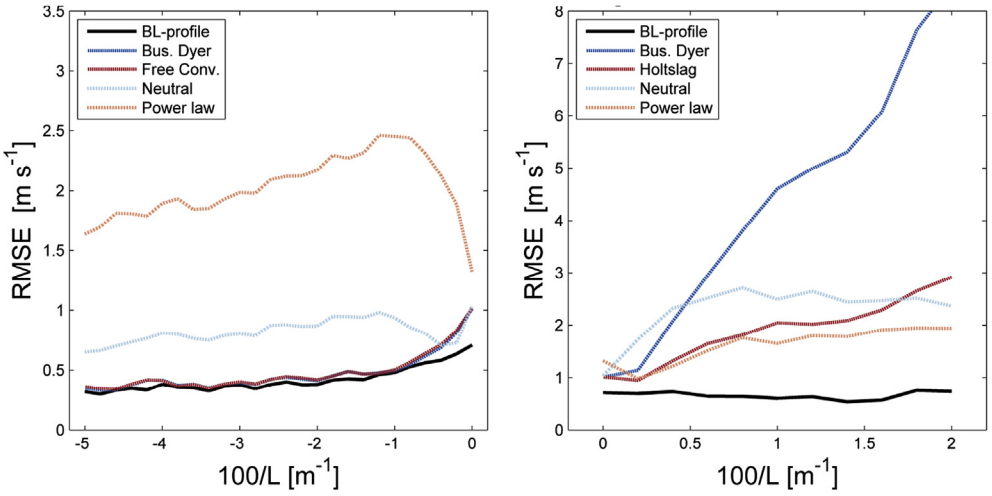

Fig. 6. RMSE of various wind profiles for unstable (left panel) and stable (right panel) conditions. The wind profiles included here correspond to the derived extended wind profile (BL-profile), the surface layer wind profile with specific stability correction functions (Bus. Dyer, Free Convection and Holtslag), the surface layer wind profile without stability correction (Neutral) and a power law wind profile with an exponent of 0.14 following [22].

5. Impact on wind turbine performance

The impact of wind shear on wind turbine performance is shown for wind turbine power production and fatigue loads separately. This assessment is done for the derived and parametrized extended wind shear profile as well as for the standard diabatic shear profile with the Businger-Dyer stability correction for stable conditions and the Free Convection correction for unstable conditions. The industry design software Bladed is used to obtain wind turbine fatigue loads from load simulations, and the fatigue loads of the blade root flapwise bending moment are assessed since blade root loads are sensitive to wind shear, in contrary to for example tower loads [20]. The NREL 5MW wind turbine [23] has been considered in this study, which is a theoretic wind turbine frequently used in wind energy research. It is outside the scope of this research to present a detailed description of the NREL 5MW wind turbine specifications, but main characteristics are a 90 m hub height and 63 m blade length. Wind shear profiles therefore must extend up to at least 153 m height to characterize shear across the rotor disc of the wind turbine. As will be shown, this is not always the case for stable conditions according to Equation (36).

5.1. Power production

It is recognised in Ref. [40] that wind shear has a profound impact on the energy flux across the rotor disc of a wind turbine, thereby influencing the power production of a wind turbine as well. This is also shown in Ref. [42] implicitly, who found that power production increases if the atmosphere has a stable stratification. In contrary however [11], show that wind turbine power production decreases when turbulence levels are low (i.e., stable conditions), which they contribute to shear effects. Similarly, in Ref. [38] it is found that wind turbine power production increases for unstable conditions and decreases for stable conditions compared to neutral conditions. In these studies however, observation data of wind turbine power production is considered, and since in practice a wind turbine is influence by both turbulence and wind shear it unclear to what extend results are caused by wind shear specifically. Due to the conflicting conclusions of the studies mentioned here, it is decided to perform an idealised simulation experiment in which solely wind shear is consider while turbulence is neglected, Though this is not representative for actual conditions, it does provide fundamental insight in the influence of wind turbine power production as a function of wind shear alone.

Following the IEC guidelines [21], the kinetic energy flux across the rotor disc of a wind turbine is defined with uniform constant wind speed across the rotor disc

$$KE = \frac{1}{2}\rho \overline{U}_h^3 A \tag{44}$$

Here ρ is the air density, A is the rotor disc area and it is assumed that the hub height wind speed $\overline{U}_h$ is a representative wind speed experienced by the wind turbine over the rotor disc area. Incorporating the effect of wind shear, one has to consider a height dependence of $\overline{U}$ and a corresponding height dependant area A

$$KE = \frac{1}{2}\rho \int \overline{U}(z)^3 A(z) dz \tag{45}$$

Note that implicitly it is assumed that the air density is constant across the rotor disc. If one divides the rotor disc area into a finite number of areas to approximate the integral with a summation, one can determine at each height z the corresponding wind speed with the derived shear profile (as a function of stability). Since the segment of a circle above a horizontal line at a distance d of the centre of the circle can be analytically calculated as

$$A_{seg} = R^2 \text{asin}\left(\frac{\sqrt{R^2 - d^2}}{R}\right) - d\sqrt{R^2 - d^2} \tag{46}$$

it follows that the area of a segment confined by two horizontal lines at a distance of respectively d_1 and d_2 of the centre of the circle equals

$$A(z) = R^2\left[\text{asin}\left(\frac{\sqrt{R^2 - d_1^2}}{R}\right) - \text{asin}\left(\frac{\sqrt{R^2 - d_2^2}}{R}\right)\right] - d_1\sqrt{R^2 - d_1^2} + d_2\sqrt{R^2 - d_2^2} \tag{47}$$

In the following assessment the shear dependant energy flux is assessed relative to uniform shear conditions. Combing Equations (44) And (45) one finds

$$KE_{\%} = 100 \sum_{z} \frac{\overline{U}(z)^3}{\overline{U}_h^3} \frac{A(z)}{\pi R^2} \quad (48)$$

where the area in Equation (44) is rewritten as πR^2 and $KE_{\%}$ is the relative kinetic energy flux that is used in the following analyses. Results are shown in Fig. 7.

It is found that for unstable and neutral conditions there is a limited difference in the relative kinetic energy flux when using either of the considered shear profiles. Besides, for such conditions the relative kinetic energy flux is always slightly less than 100%, and it is found to vary between 98.2 and 99.8%. This is in agreement with the results found by Ref. [40] who showed that for low wind shear, which corresponds to unstable and neutral conditions, the relative kinetic energy flux is less than 100%. For stable conditions however there is a significant difference in the results obtained depending on the shear profile considered. If one determines the relative kinetic energy flux with the diabatic surface layer shear profile, one finds that for stable conditions the relative kinetic energy flux is well above 100% with a maximum of 109.5% for high wind speeds. If one however considers the extended wind shear profile, one finds a relative kinetic energy flux well below 100% with a minimum of 93%. Combined, this results in a difference of 15% in the relative kinetic energy flux depending on the shear profile considered. For low wind speeds and stable conditions, the relative kinetic energy flux is not computed for the extended shear profile in Fig. 7. For such conditions, Equation (36) determines h below the maximum blade tip height, hence the shear profile cannot be computed up to the maximum blade height. This is a drawback of the shear profile derived in this study, since for low wind speeds and stable conditions one cannot determine a representative wind shear profile, and thus power production and fatigue load assessment cannot be carried out. This shows that for offshore conditions it is necessary to consider the inversion layer at the top of the boundary layer, and possibly even free atmospheric conditions above the boundary layer.

Based on earlier findings shown in Fig. 4, one can conclude that the proposed extended wind shear profile indeed results in a reduction in wind shear compared to the surface layer diabatic shear profile, however the shear profiles in Fig. 4 do not have similar hub height wind speeds for a given stability. As such, to better understand the difference found in the relative kinetic energy flux, Fig. 8 shows a comparison of wind shear profiles for a fixed hub height wind speed of 16 m s^{-1}. It is shown that for unstable conditions differences between the two shear profiles considered are small. For stable conditions the extended shear profile results in an increase in wind speed below hub height compared to the surface layer shear profile, and a decrease in wind speed above hub height compared to the surface layer shear profile. Since the kinetic energy flux is proportional to the wind speed cubed, the kinetic energy flux calculated by the surface layer shear profile is higher than the kinetic energy flux determined with the extended shear profile.

Though this explains the differences found in Fig. 7, the results obtained with the extended shear profile deviate significantly from the results obtained in Refs. [40] and [42]. Strong wind shear occurs for stable conditions, and where in Fig. 7 it is shown that for stable conditions the kinetic energy flux decreases, both [40] and [42] show that for stable conditions the power production of a wind turbine increases. This difference can be explained in various ways. First of all, the power production of a wind turbine does not equal the kinetic energy flux determined here but also depends on the efficiency of the turbine to extract power from the wind. The theoretic maximum efficiency of a wind turbine, known as the Betz-Joukowsky limit, depends on wind shear and for neutral conditions [8] show differences in the Betz-Joukowsky limit of 1–2% due to changes in surface roughness. Similarly, for non-neutral conditions it is expected that the theoretic maximum efficiency of a wind turbine will depend on atmospheric stability. Besides, both [40] and [42] consider wind shear in terms of a power law, which results in fundamentally different shear profiles compared to those derived here. In Fig. 8 it is shown that for stable conditions wind shear is indeed strong but primarily close to the surface below hub height. Since the boundary layer is shallow (it is 179 m for the stable profiles in Fig. 8), above hub height wind shear diminishes rapidly with height. In both [40] and [42] shear is considered with a power law with a fixed power, thereby keeping wind shear high above the hub height as well. The rapid decrease in wind shear above hub height due to the parametrization of h (i.e., a shallow boundary layer for stable conditions), is likely causing the major difference in the kinetic energy flux for stable conditions. Besides, note as well that [42] consider power curves as a function of a rotor disc equivalent wind speed, which depends on wind shear. It is mentioned in Ref. [42] that they "found a higher rotor-averaged wind speed than hub-height wind speed under stable conditions, and consequently greater energy production". Since in

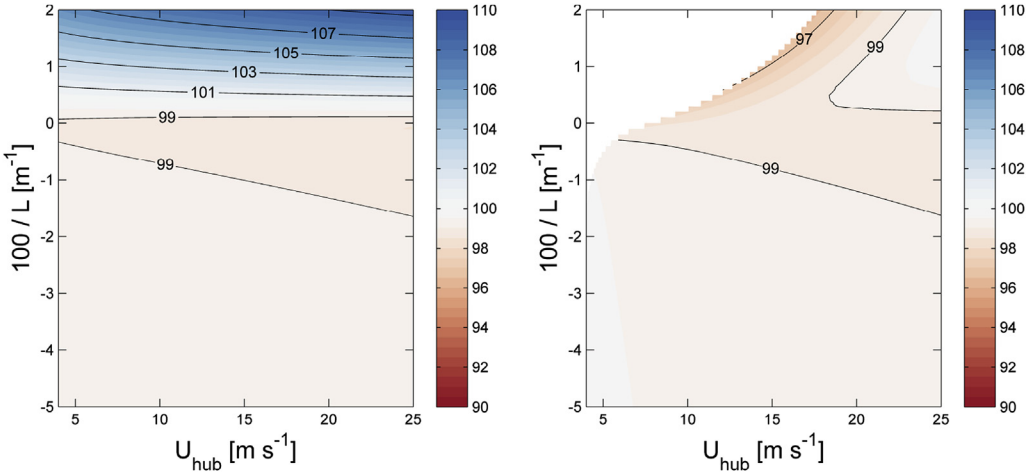

Fig. 7. Relative kinetic energy flux assuming the conventional diabatic wind shear (left panel) and assuming the derived and parametrized extended wind shear profile (right panel) for a given hub height wind speed and atmospheric stability.

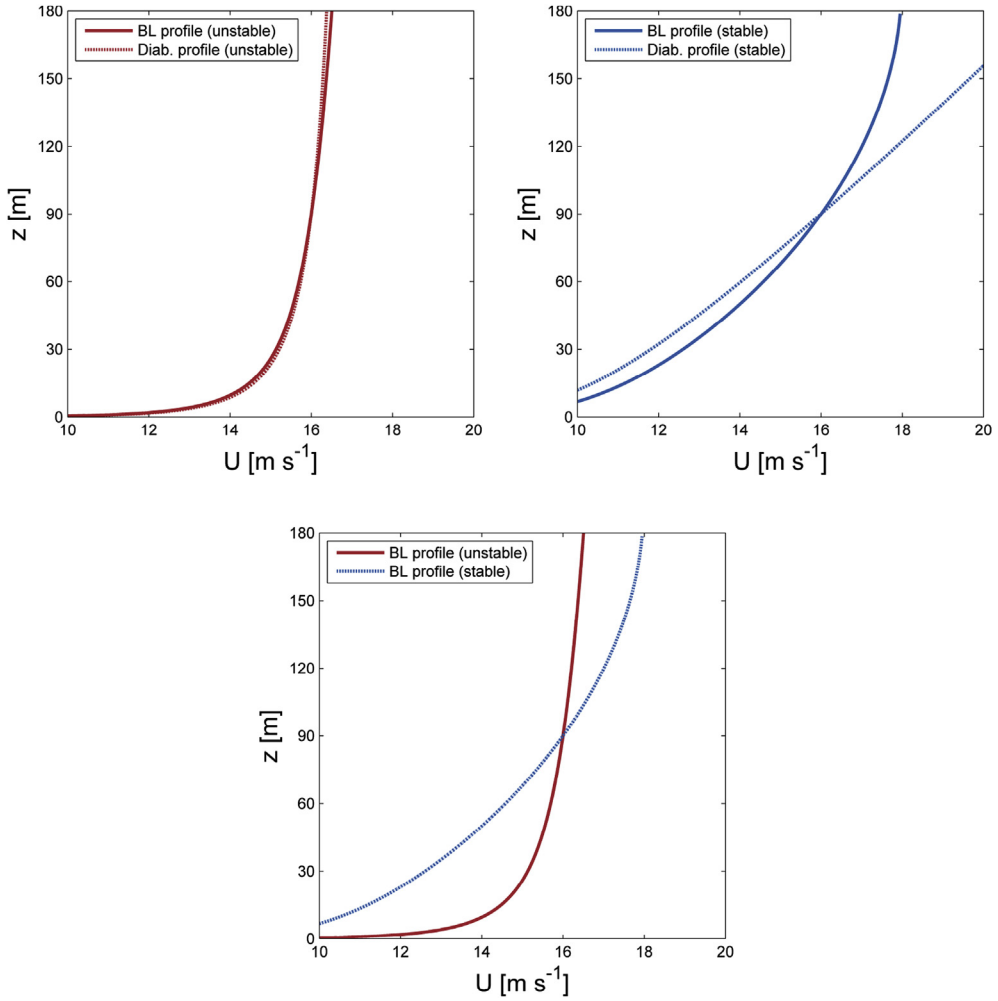

Fig. 8. Example shear profiles with $\overline{U}(z_{hub}) = 16$ m s^{-1} for unstable ($L = -100$ m, upper left panel) and stable ($L = 100$ m, upper right panel) conditions. The lower panel directly compares the extended shear profile for unstable an stable conditions.

this study the hub height wind speed is kept constant (and thus the equivalent wind speed differs for stable and unstable conditions), results will by default differ from those presented in Ref. [42].

5.2. Fatigue loads

Lifetime fatigue loads are expressed in terms of equivalent loads (see Ref. [18] for details) for comparison purposes with other studies. The impact of specific shear models on wind turbine fatigue loads is compared to the work of Sathe, who assessed the influence of shear on wind turbine fatigue loads both without considering turbulence [31] as well as with turbulence [33]. The results found in this study are shown in Fig. 9.

In absence of turbulence, results shown for the surface layer shear profile (left panel of Fig. 9) correspond qualitatively to those shown in Ref. [31]. For a given hub height wind speed fatigue loads tend to decrease slightly for unstable conditions compared to neutral conditions, and loads increase significantly for stable conditions. If one considers the derived extended wind shear profile, fatigue loads tend to decrease significantly for stable conditions compared to using the surface layer shear profile, which is shown for high wind speeds only in Fig. 9. This agrees with the results presented in Fig. 4 where for stable conditions it is shown that the surface layer profile significantly overestimated wind shear between 50 and 150 m height.

To place these results in perspective, one can find that for high wind speeds and stable conditions the surface layer wind shear profile results in an increase in fatigue loads by 85%. This percentage is significantly higher compared to the maximum of 6% presented in Refs. [33]; however note that in their study besides wind shear also turbulence characteristics where considered as well as the frequency of occurrence of a given combination of atmospheric stability and hub height wind speed. Besides, the offshore atmosphere considered in this study is found to be predominantly unstable or neutral stratified [18], and for these conditions differences in fatigue loads between both shear profiles are less than 1% in Fig. 9, which is more in line with the results of [33]. As such, the error introduced in load simulation by wrongly assuming validity of the surface layer shear profile up to the maximum blade tip height is likely significantly smaller than the maximum of 85% found in this study. Still, the results shown here do indicate that shear induced loads (in contrary to turbulence induced loads) are significantly smaller than one might find by wrongly assuming validity of the surface layer shear profile for the entire boundary layer.

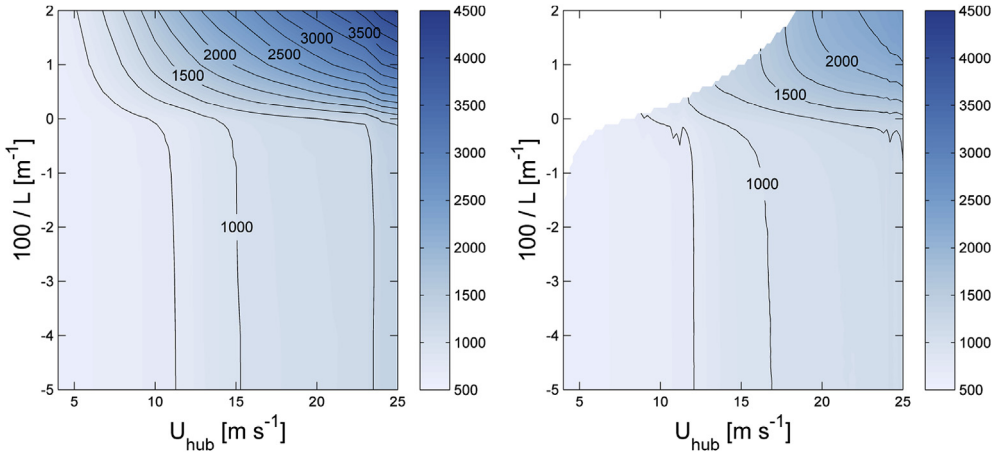

Fig. 9. Similar as Fig. 7 but for the equivalent fatigue load of the blade root flapwise moment in kNm.

6. Discussion

In this paper we have parametrized Gryning's boundary layer shear profile for an offshore site, and put it into perspective of wind energy. The advantageous outcome is that we have specifically parametrized the wind profile as a continuous function of atmospheric stability, however, due to limitations in the available observation data it has not been possible to validate the wind profile up to the top of the boundary layer. It has been shown that for stable conditions the wind profile decreases in accuracy in close proximity of the top of the boundary layer (that is, the parametrized estimate of the boundary layer height). For unstable conditions however the accuracy of the wind profile in close proximity of the top of the boundary layer has not been assessed in detail since observation data is used up to 315 m height at most. As such, it would be useful to perform similar research with offshore observation data that reaches substantial higher altitudes. Ideally one would also have access to observation data at higher altitudes that can be used as indication of the height of the boundary layer.

Due to the scope of this research we have validated the wind profile for a single observation site, hence the general applicability of the wind profile at offshore sites is not known. It is therefore strongly recommended to assess at other offshore sites if the wind profile can be validated up to the top of the boundary layer height. Though there are no physics based arguments that limit the applicability of Gryning's wind profile to the specific site considered in this study, it is well possible that parametrizations adopted are site specific.

Lastly, it is expected that the influence of adopting specific wind profiles on wind turbine performance is likely wind turbine specific. The reference wind turbine considered in this study has a 90 m hub height and a 63 m blade length, hence the blades experience changing wind conditions between 27 and 153 m height. If we would alter the turbine dimensions however, the blades encounter changing wind conditions at different altitudes, which might influence the subsequent response of the wind turbine to the wind. As such, it would be beneficial to assess for several wind turbines with different dimensions how wind shear influences wind turbine performance.

7. Conclusions

Given the ongoing trend to scale up wind turbines to greater dimensions, the validity of traditional surface layer wind shear models in wind energy research is questioned. Especially offshore, where the atmospheric boundary layer is typically shallow compared to onshore sites, logarithmic shear profiles are not valid up to the hub height, let alone up to the maximum blade tip height. A new shear profile based on the wind shear profile of Gryning is derived that is valid not only in the surface layer but for the entire atmospheric boundary layer.

The wind shear profile depends on specific parametrizations of the resistance functions A and B and the boundary layer depth h. A combination of the resistance functions of Byun and the Rossby-Montgommery parametrization of h has resulted in an analytically integratable wind gradient that is a continuous function of atmospheric stability in terms of the Obkuhov length L. For the constant c that is introduced by the Rossby-Montgommery parametrization it is found that c is strongly dependant on atmospheric stability, and ranges from 0.04 (very stable) to 0.17 (very unstable) with a value of 0.09 for neutral atmospheric stratification. These values are significantly lower compared to results found in literature, specifically for neutral and stable conditions.

Based on two years of observation data taken from the offshore meteorological mast IJmuiden, it is found that the derived and parametrized extended wind shear profile outperforms traditional surface layer shear profiles for neutral and (very) stable conditions. Especially for strong stable conditions, for which shallow boundary layers occur, the validity of traditional logarithmic shear profiles is limited to the lowest 40 m. This limits the applicability of these commonly used surface layer wind shear profiles for wind energy research. The derived shear profile has significantly lower root mean square errors for stable conditions compared to the surface layer shear profiles.

The impact of using the derived extended shear profile in wind energy is explored by considering the power production and blade root fatigue loads experienced by a reference turbine. It is found that for unstable and neutral stratification changing the wind shear profile to the derived extended shear profiles results in limited differences in both the kinetic energy flux and the blade root fatigue loads experienced by the wind turbine. For stable stratifications however there are significant differences. With respect to the fatigue loads, one will overestimate blade root fatigue loads by nearly a factor 2 if one considered the surface layer shear profile. This is caused by the overestimation of wind shear by the Businger-Dyer stability correction function frequently used to correct the logarithmic wind shear profile for stable conditions. For power production it is also found that the kinetic energy flux through the rotor disc is overestimated if one considers the surface layer shear model. The reduction in the energy flux found by using the

extended wind shear profile is caused by a decrease in wind shear above the wind turbine hub height for stable conditions. Compared to the kinetic energy flux determined with a uniform wind speed across the rotor disc, results are opposite for the two shear profiles compared and while for the surface layer shear profile the kinetic energy flux increases by up to 9% for stable conditions, the extended shear profile actually results in a reduction in the kinetic energy flux by up to 6%.

It is also found that for low and moderate wind speeds (less than 15 m s^{-1} typically), the adopted parametrization of the boundary layer height is frequently lower than typical maximum blade tip heights. For such conditions one cannot accurately describe shear across the entire rotor disc. This indicates that, in the offshore environment, large wind turbines might frequently experience free atmospheric conditions at the maximum blade tip height depending on the frequency of occurrence of strong stable stratification.

Acknowledgements

This research is funded by the FLOW-project (Far and Large Offshore Wind). We would like to thank ECN (Energy Research Centre of the Netherlands) for providing all data used in this research.

References

[1] E. Akylas, M. Tombrou, Interpolation between businger-dyer formulae and free convection forms: a revised approach, Boundary-Layer Meteorol. 115 (2005) 381–398.
[2] P. Baas, G.J. Steeneveld, B.J.H. van de Wiel, A.A.M. Holtslag, Exploring self-correlation in stably stratified conditions, J. Atmos. Sci. 63 (2006) 3045–3054.
[3] A.C.M. Beljaars, A.A.M. Holtslag, Flux parameterization over land surfaces for atmospheric models, J. Appl. Meteorol. 30 (1991) 327–341.
[4] A.K. Blackader, The vertical distribution of wind and turbulent exchange in a neutral atmosphere, J. Geophys. Res. 67 (1962) 3095–3102.
[5] A.K. Blackader, H. Tennekes, Asymptotic similarity in neutral barotrophic planetary boundary layers, J. Atmos. Sci. 25 (1968) 10151020.
[6] J.A. Businger, J.C. Wyngaard, Y. Izumi, E.F. Bradley, Flux-profile relationships in the atmospheric boundary layer, J. Atmos. Sci. 28 (1971) 181–189.
[7] D.W. Byun, Determination of similarity functions of the resistance laws for the planetary boundary layer using surface-layer similarity functions, Boundary-Layer Meteorol. 57 (1991) 17–48.
[8] L.P. Chamorro, R.E.A. Arndt, Non-uniform velocity distribution effect on the betz-joukowsky limit, Wind Energy 16 (2013) 279–282.
[9] H. Charnock, Wind stress on a water surface, Q. J. R. Meteorol. Soc. 81 (1955) 639.
[10] Y. Cheng, W. Brutsaert, Flux-profile relationships for wind speed and temperature in the stable atmospheric boundary layer, Boundary-Layer Meteorol. 114 (2005) 519–538.
[11] D.L. Elliot, J.B. Cadogan, Effects of wind shear and turbulence on win dturbine power curves, in: Proceedings of the 1990 European Community Wind Energy Conference and Exhibition, 1990.
[12] C.W. Fairall, E.F. Bradley, D.P. Rogers, J.B. Edson, G.S. Young, Bulk parameterization of air-sea fluxes for tropical ocean global atmosphere coupled-ocean atmosphere response experiment, J. Geophys. Res. 101 (1996) 3747–3764.
[13] A.A. Grachev, C.W. Fairall, Dependence of the Monin-Obukhov stability parameter on the bulk Richardson number over the ocean, J. Appl. Meteorol. 36 (1997) 406–414.
[14] S. Gryning, E. Batchvarova, B. Brümmer, H. Jorgensen, S. Larsen, On the extension of the wind profile over homogeneous terrain beyond the surface boundary layer, Boundary-Layer Meteorol. 124 (2007) 251–268.
[15] K.S. Hansen, G.C. Larsen, S. Ott, Dependence of offshore wind turbine fatigue loads on atmospheric stratification, J. Phys. Conf. Ser. 524 (2014) 012165, http://dx.doi.org/10.1088/1742–6596/524/1/012165.
[16] D.A. Haugen, J.C. Kaimal, E.F. Bradley, An experimental study of Reynolds stress and heat flux in the atmospheric surface layer, Q. J. R. Meteorol. Soc. 97 (1971) 168–180.
[17] U. Högström, Non-dimensional wind and temperature profiles in the atmospheric boundary layer: a re-evaluation, Boundary-Layer Meteorol. 42 (1988) 55–78.
[18] M.C. Holtslag, W.A.A.M. Bierbooms, G.J.W. van Bussel, Definition of the equivalent atmospheric stability for wind turbine fatigue load assessment, J. Phys. Conf. Ser. 524 (2014) 012110, http://dx.doi.org/10.1088/1742–6596/524/1/012110.
[19] M.C. Holtslag, W.A.A.M. Bierbooms, G.J.W. van Bussel, Validation of surface layer similarity theory to describe far offshore marine conditions in the Dutch North Sea in scope of wind energy research, J. Wind Eng. Industrial Aerodynamics 136 (2015) 180–191.
[20] M.C. Holtslag, W.A.A.M. Bierbooms, G.J.W. van Bussel, Wind turbine fatigue loads as a function of atmospheric conditions offshore, Wind Energy (2016), http://dx.doi.org/10.1002/we.1959 (n/a–n/a).
[21] 'IEC', Iec 61400–1 ed.3: Wind-turbines – Part 1: Design Requirements, Tech. Rep., International Electrotechincal Commission, 2005.
[22] 'IEC', Iec 61400–3 ed.1: Wind-turbines – Part 3: Design Requirements for Offshore Wind Turbines, Tech. Rep., International Electrotechincal Commission, 2009.
[23] J. Jonkman, S. Butterfield, W. Musial, G. Scott, Definition of a 5-MW Reference Wind Turbine for Offshore Systemd Evelopment, Tech. Rep., National Renewable Energy Laboratory, 2009.
[24] B. Lange, S. Larsen, J. Hojstrup, R. Barthelmie, The influence of thermal effects on the wind speed profile of the coastal marine boundary layer, Boundary-Layer Meteorol. 112 (2004) 587–614.
[25] A.S. Monin, A.M. Obukhov, Basic laws of turbulent mixing in the ground layer of the atmosphere, Tr. Akad. Nauk. SSSR Geophiz. Inst. 151 (1954) 163–187.
[26] A.M. Obukhov, Turbulence in the atmosphere with a non-uniform temperature, Boundary-Layer Meteorol. 2 (1971) 7–29.
[27] C.A. Paulson, The mathematical representation of wind speed and temperature profiles in the unstable atmospheric surface layer, J. Appl. Meteorol. 9 (1970) 857–861.
[28] A. Peña, S. Gryning, Charnock's roughness length model and non-dimensional wind profiles over the sea, Boundary-Layer Meteorol. 128 (2008) 191–203.
[29] A. Peña, S. Gryning, C.B. Hasager, Comparing mixing-length models of the diabatic wind profile over homogeneous terrain, Theor. Appl. Climatol. 100 (2010a) 325–335.
[30] A. Peña, S. Gryning, J. Mann, C.B. Hasager, Length scales of the neutral wind profile over homogeneous terrain, J. Appl. Meteorol. Clim. 49 (2010b) 792–806.
[31] A. Sathe, W. Bierbooms, Influence of different wind-profiles due to varying atmospheric stability on the fatigue life of wind turbines, J. Phys. Conf. Ser. 75 (2007) 012056, http://dx.doi.org/10.1088/1742–6596/75/1/012056.
[32] A. Sathe, S.E. Gryning, A. Peña, Comparison of the atmospheric stability and wind profiles at two wind farm sites over a long marine fetch, Wind Energy 14 (2011) 767–780.
[33] A. Sathe, J. Mann, T. Barlas, W.A.A.M. Bierbooms, G.J.W. van Bussel, Influence of atmospheric stability on wind turbine loads, Wind Energy 16 (2013) 1013–1032.
[34] A.R. Sathe, Influence of Wind Conditions on Wind Turbine Loads and Measurement of Turbulence Using Lidars, Ph.D. thesis, Technical University Delft, 2012.
[35] R.B. Stull, An Introduction to Boundary Layer Meteorology, Kluwer Acadmic Publishers, 1988.
[36] A.P. van Ulden, J. Wieringa, Atmospheric boundary layer research at Cabauw, Boundary-Layer Meteorol. 78 (1996) 39–69.
[37] A.J.M. van Wijk, A.C.M. Beljaars, A.A.M. Holtslag, W.C. Turkenburg, Evaluation of stability corrections in wind speed profiles over the north sea, J. Wind Eng. Industrial Aerodynamics 33 (1990) 551–566.
[38] B.J. Vanderwende, J.K. Lundquist, The modification of wind turbine performance by statistically distinct atmospheric regimes, Environ. Res. Lett. 7 (2012), 034035 (7pp).
[39] D. Vickers, L. Mahrt, Observations of non-dimensional wind shear in the coastal zone, Q. J. R. Meteorol. Soc. 125 (1999) 2685–2702.
[40] R. Wagner, M. Courtney, J. Gottschall, P. Lindelöw-Marsden, Accounting for speed shear in wind turbine power performance measurement, Wind Energy 14 (2011) 993–1004.
[41] E.J. Werkhoven, J.P. Verhoef, Offshore Meteorological Mast IJmuiden – Abstract of Instrumentation Report, February 2012. ECN, ECN-WindMemo-12–010, ECN project nr.:5.1008.
[42] S. Wharton, J.K. Lundquist, Atmospheric stability affects wind turbine power collection, Environ. Res. Lett. 7 (2012), 014005 (9pp).
[43] S.S. Zilitinkevich, J.W. Deardoff, Similarity theory for the planetary boundary layer of time-dependent height, J. Atmos. Sci. 31 (1974) 1449–1452.